Reflection processing of synthetic crosshole seismic data

Ashraf A. Abdalla and Robert R. Stewart

ABSTRACT

Crosshole seismic reflection processing is demonstrated in this research work. Reflected upgoing and downgoing wavefields are studied here with respect to their geometrical concepts and exploration applications. Conventional processing techniques are followed to separate the two wavefields. Unlike Vertical Seismic Profiling (VSP) processing, downgoing primary reflections are selected and processed to contribute with the upgoing reflections in obtaining a subsurface image for the media between the boreholes. As in VSP processing, crosshole data are transformed into surface distance and subsurface depth domain. This method was first applied in 1984 with a constant velocity model assumption. Here, we contribute the multi-layered model and derive the analytical solution of the constant velocity transformation (XHL-CDP Transformation). A subsurface image is obtained by summing multiple transformed records. Depth migration is also applied to provide a correlation with the mapped data. Crosshole geometry is shown to have an extended subsurface coverage between the boreholes which delineates the horizon lateral continuity and complements the interpretation of well logs and VSP data.

INTRODUCTION

Crosshole seismic data are acquired by emitting seismic energy from sources deployed in one borehole at some depths and recording the resulting energy on receivers placed in another borehole.

Most crosshole studies have used the direct arrivals to obtain velocity information about the medium between the boreholes using tomographic inversion techniques. Of these studies, Ivansson (1985) estimated seismic velocities for a two-dimensional (2-D) model in the presence of low-velocity zones. Macrides (1987) compared seismic velocities before and after a steam injection experiment. Bregman et al., (1989) obtained a 2-D model of the compressional seismic velocity between two boreholes at a fire-flood site.

A few studies have considered the different types of scattered waves which constitute the later arrivals in a crosshole seismic record. Reflected, transmitted, guided and converted waves are all prominent in crosshole data (Hu et al., 1988b). Acoustic modelling and imaging of crosshole data with finite-differences were presented by Hu et al. (1988a), for common-source gathers (prestack), and by Zhu and McMechan (1988), for stacked data. In those studies, the reverse-time wave equation method was used to obtain a depth section from the total wavefield. Another 2-D migration/inversion technique by Beydoun et al. (1988) produced elastic (velocity and density) maps of the subsurface from the full waveform.

Crosshole seismic data in the kilohertz range can resolve vertical layers as thin as 1.5 m. The loss of these high frequencies can be minimumed since the entire experiment is placed beneath the attenuative weathered layer. So, we can see that the two important interrelated factors, data frequency and target depth, in seismic resolution are perhaps less of a problem in the crosshole environment. Iverson (1988) discussed seismic resolution and its relation with Fresnel zone horizontally and with the seismic wavelength vertically.

In this study, we discuss the subsurface coverage and the reflection processing of crosshole data. We use synthetic data for their simplicity and known solution as a preliminary research to validate our derivations and processing approaches.

GEOMETRY AND METHOD

A simple crosshole geometry is presented in Figure 1. A flat multi-layered model in which velocity increases with depth is shown. Only one source at depth is shown. In real practice, we would have many sources scanning the zone of interest. There is a set of recorders placed in the receiver borehole to detect the arriving signal. P-wave ray path examples are shown for direct arrivals D, reflected upgoing RU, and reflected downgoing arrivals RD. Note that downgoing arrivals can be primary reflections.
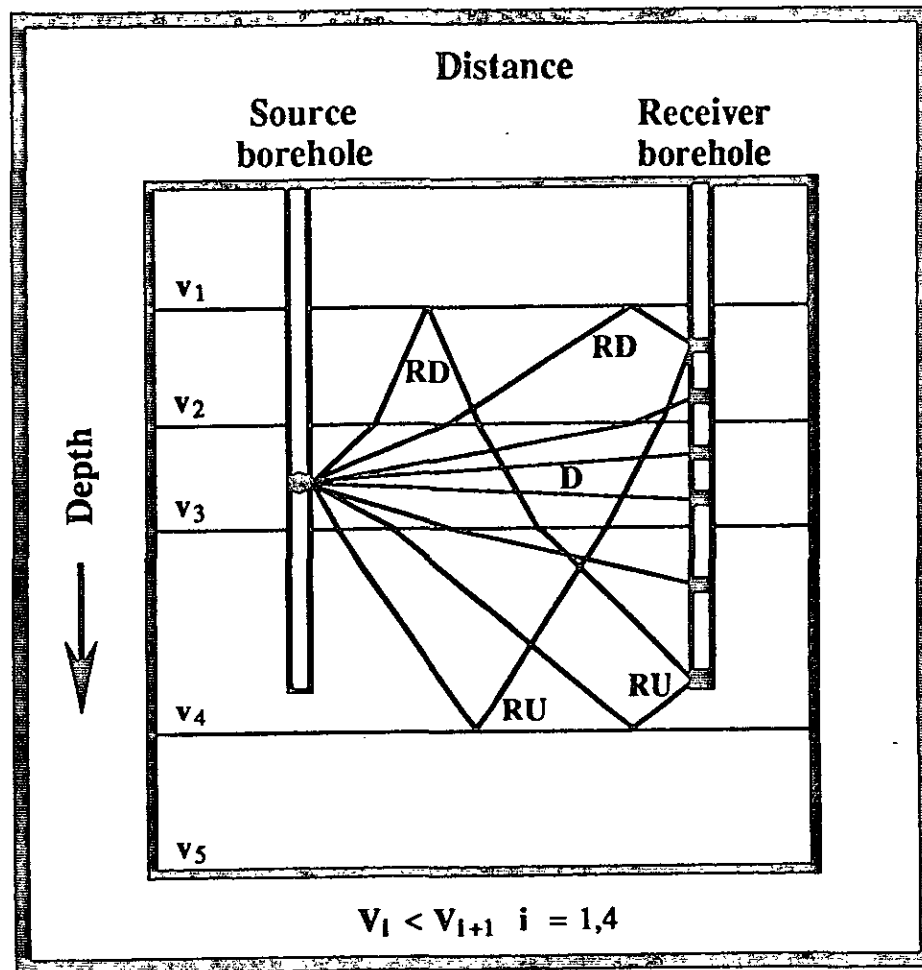

Figure 1: Geometry of the crosshole experiment. **D** represents the direct arrival, **RU** and **RD** represent reflected upgoing and downgoing respectively.

Our study considers both reflected wavefields, upgoing and downgoing, to obtain a 2-D image of the medium between the two boreholes using conventional CDP and VSP processing. This method was introduced by Baker and Harris (1984) and followed by Iverson (1988). A one-layer (constant-velocity) model was a major assumption in the

previous studies. Here, we consider the multi-layered model with its proper transformation attributes, depth, 2-way normal incidence time and reflection point location (offset).

NUMERICAL MODELLING

A geologic model is defined here based on an experiment conducted in the Midale field of southeastern Saskatchewan by Shell Canada. Figure 2 shows the depth model identifying all the interfaces as I1, I2, I3, ..., I9 and their corresponding depths. The P-wave velocity for each layer is also displayed on the same figure. Note that the distance along the top of the model and the depths of interfaces are relatively located as the real geometry dimensions. The distance between the boreholes is 45 m. Recorder locations, in Receiver Borehole, are at depths from 96 to 158 m with 2 m interval (32 receivers). There are three shots, numbered 1 to 3, at depths 100, 124 and 180 m respectively placed in Source Borehole.
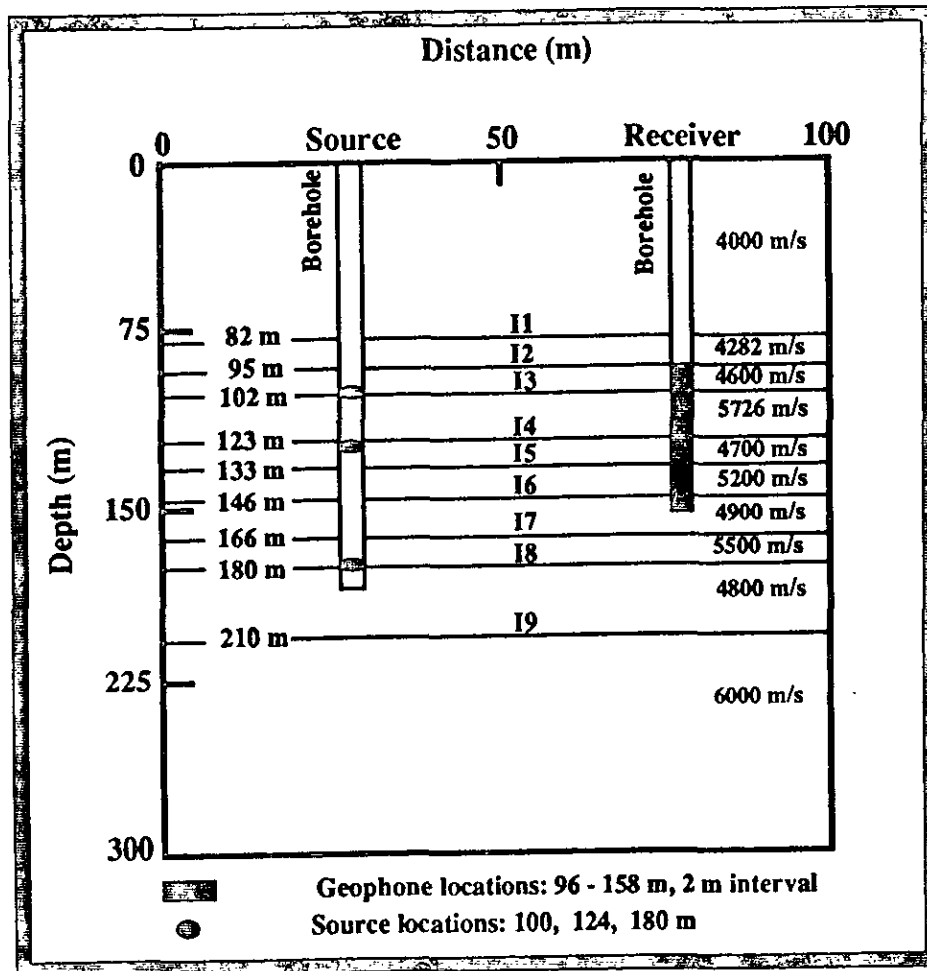

Figure 2: Depth model for generating synthetic data. Interface depths, P-wave layer velocities and array geometry are displayed on the model.

227

A ray tracing software package (Uniseis) was used to generate synthetic records for the three shots described above. A zero phase (Ricker) wavelet was convolved with the amplitude spikes produced from raytracing. The sampling interval to obtain the best event resolution and wavelet shaping was found and used as $100\ \mu s$. The wavelet was 2 ms long and had 1000 Hz of centre frequency. P-wave arrivals were measured as vertical displacements. The three simulated synthetic shots are displayed in Figure 3. Direct arrivals are labeled D, while upgoing reflections are labeled according the interface they reflected from. For example, upgoing reflections from interface 1 (I1) are given RU1 and so on for all interface reflections. The same scheme was followed for the downgoing reflections.

Due to software limitations of processing data with such small sampling interval ($100\ \mu s$), a scale factor of 10x was used. This scale factor does not affect any of our results. For example, a time of 50 ms would be scaled to appear as 500 ms in software. A velocity of 5000 m/s would appear as 500 m/s and a frequency of 1000 Hz appears as 100 Hz.

DATA PROCESSING AND DISCUSSION

One goal in this study is to show that crosshole data can generally be processed using conventional VSP processing software. When needed, computer programs can be written to treat specific processing steps. This makes crosshole processing immediately available since VSP software is very common nowadays. We also show the extended subsurface coverage of the crosshole geometry.

Because we are measuring the vertical displacement on the recording locations, we see that the direct arrivals have an increasing amplitude inversely proportional to the incidence angle θ. Figure 4 shows a schematic configuration of this phenomena for straight ray path in the case of shot 1 (Figure 3 (a)). we see that the recorder location that has the same depth as the source has a very small direct amplitude since the angle of incidence θ_2 in this case is theoretically 90°. For the top and bottom recording locations, we see that the absolute direct amplitude for the bottom location is much larger than that of the top one since $\theta_3 < \theta_1$. Now, from θ_2 to θ_1 and from θ_2 to θ_3, the absolute vertical displacement increases with decreasing incidence angle. For bending ray path, the same behavior still holds with slightly different incident angles. The same idea is applicable in shots 2 and 3 with the remark that shot 2 does not show the small direct displacement on the recorders at and around the shot depth because of the interfering downgoing reflected event from interface I4 with these direct arrivals. With that analysis established, geometrical spreading cannot be corrected for in this data using the conventional direct arrival decay. No gain of any type is applied to this data at any processing step. The values are simply brought up to a certain dB level to obtain a reasonable plot.

The processing flow of the present work is presented in Figure 5. There was no preprocessing step as deconvolution or velocity filtering in that flow since the synthetic data only contain primary events. This is an ideal situation where new methods are firstly experimented and validated. In field data situation, detailed analysis must be developed for the preprocessing stage to treat the different noise problems. For example, the removal of tube waves generated from both the source and receiver boreholes.
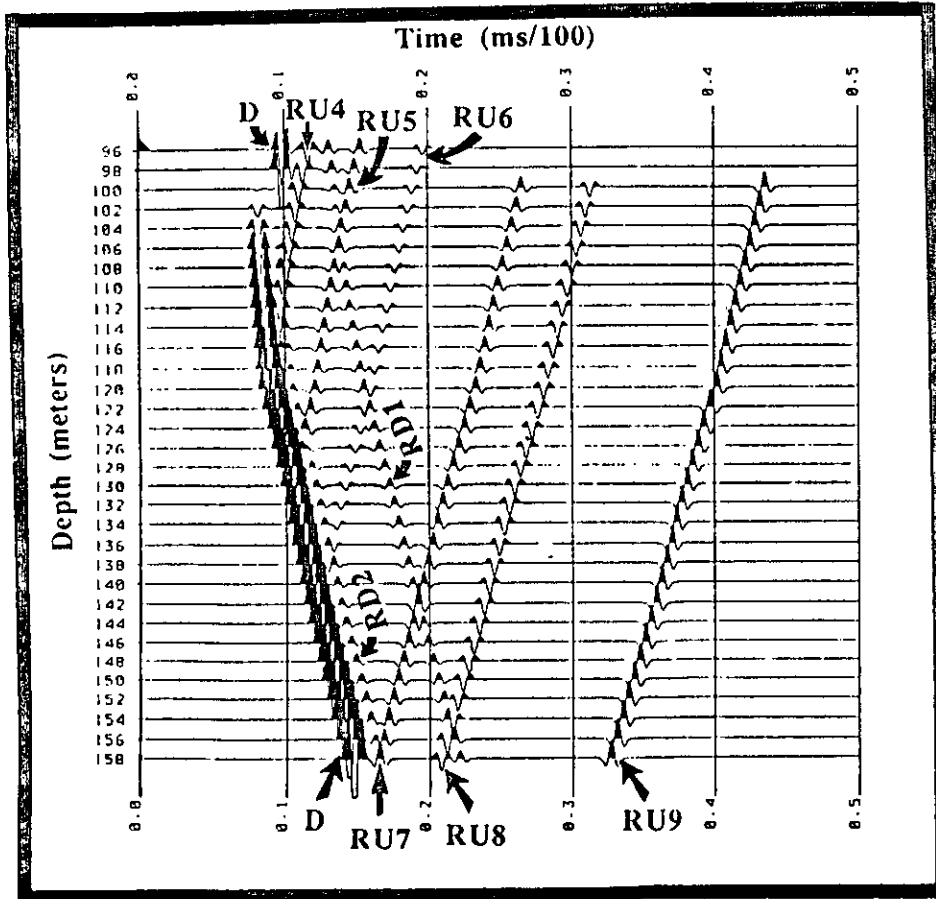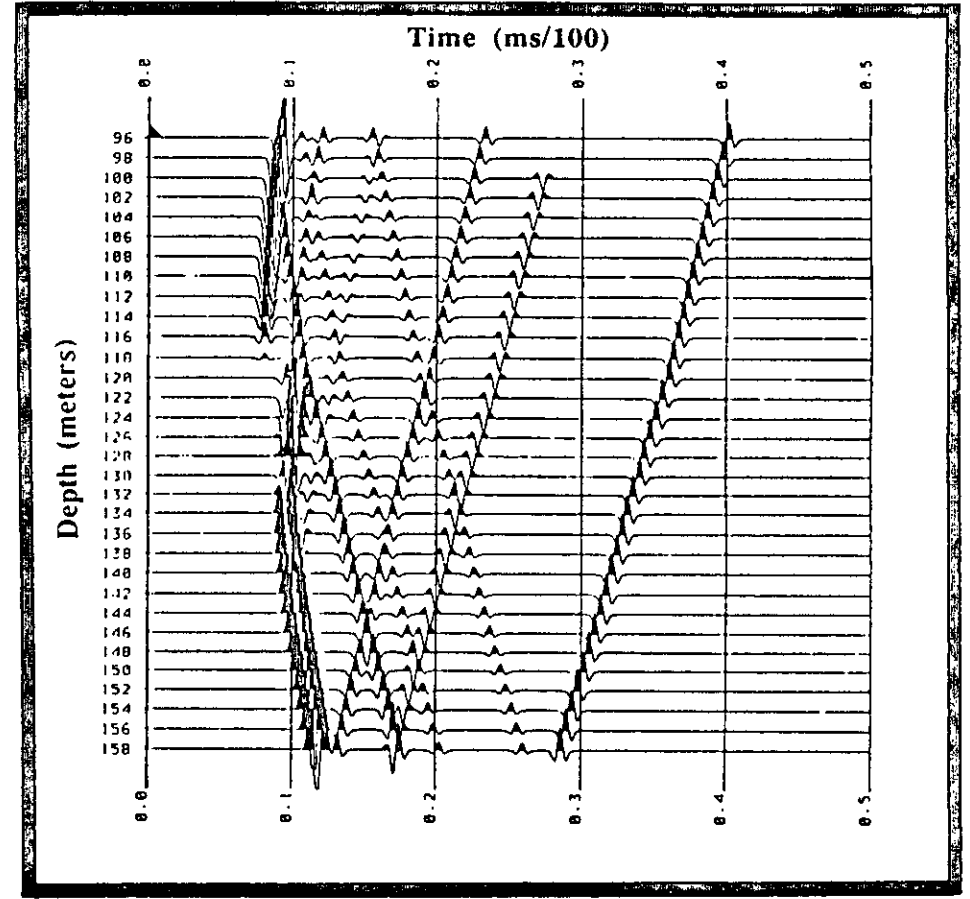
Figure 3: Synthetic shot records. a) Shot 1 at depth 100 m with geophone locations 96 to 158 m with 2 m interval (same set of geophone for every shot). Direct arrivals are labeled D, while Reflected Upgoing events are identified by RUI where I is the interface number they reflected from. Reflected Downgoing events follow the same scheme. b) Shot 2 at depth 124 m. c) Shot 3 at depth 180 m.
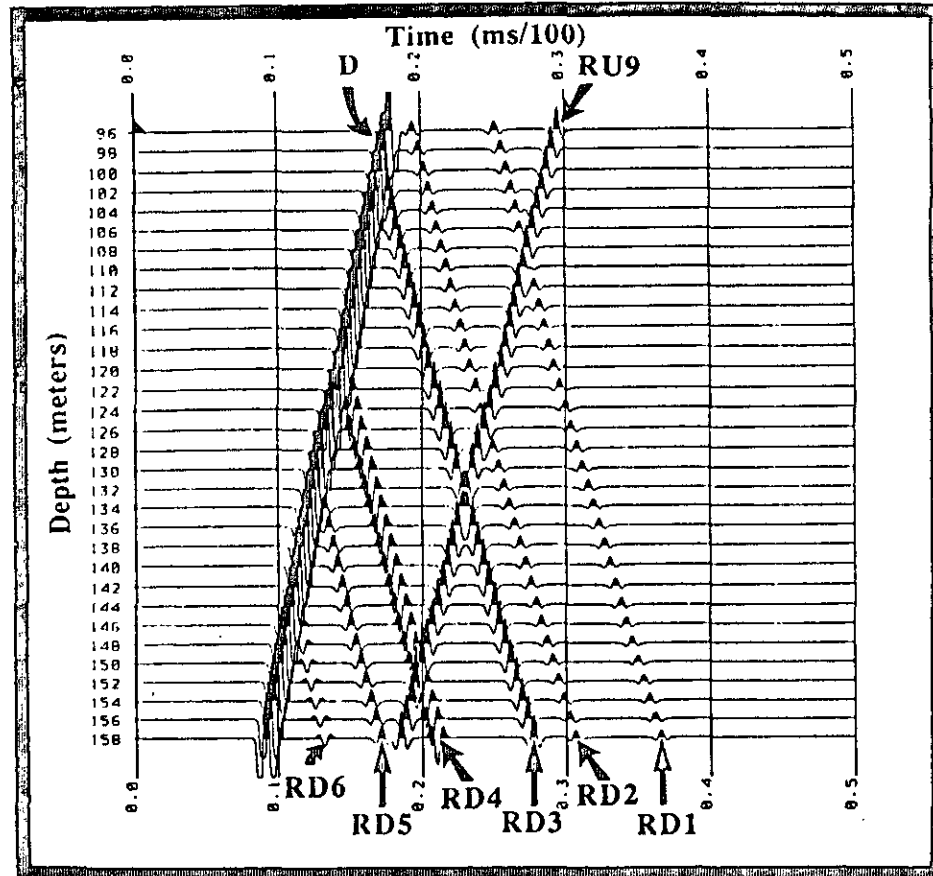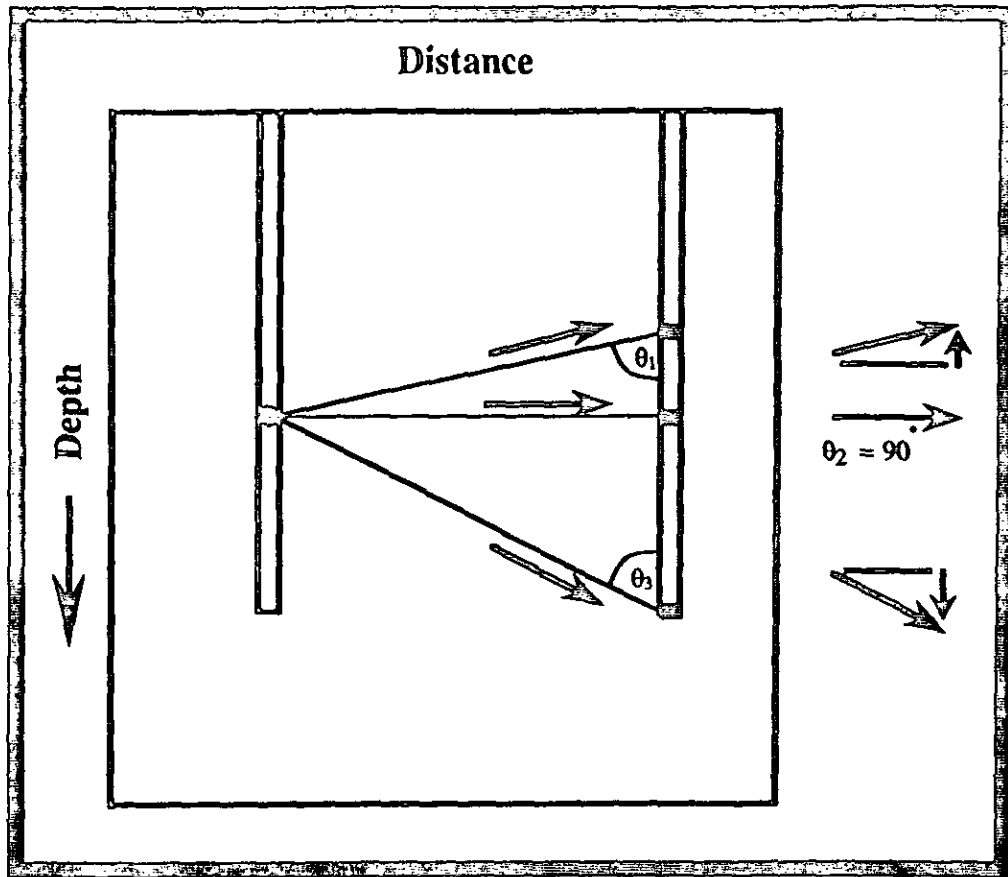
(c)

Figure 4: Direct arrival incidence angles and their relation with vertical component displacement. Note that $\theta_1 > \theta_3$.

Each shot is processed independently to the step where an image is produced for each individual shot . Then all similar-type images are summed together to produce one final image of the subsurface. The following is a description of our processing steps and their implications:

1.Input: The three shot records (Figure 3) are processed separately (as in conventional VSP processing). To test the methods, we selected only the upgoing waves in shot 1 (Figure 3 (a)), both upgoing and downgoing waves in shot 2 (Figure 3 (b)) and only downgoing waves in shot 3 (Figure 3 (c)).

2.Mute: The direct arrivals are muted out in this processing flow. No velocity information was obtained by tomographic inversion. Sonic log information was used instead to construct a background model. Nevertheless, a tomographic inversion technique would be a good check for that model. Other reasons for muting the direct arrivals are that they cause a smear in the reconstruction if left and they cannot be used in separating the wavefields since they follow a different slope from that of the reflected downgoing or upgoing events.
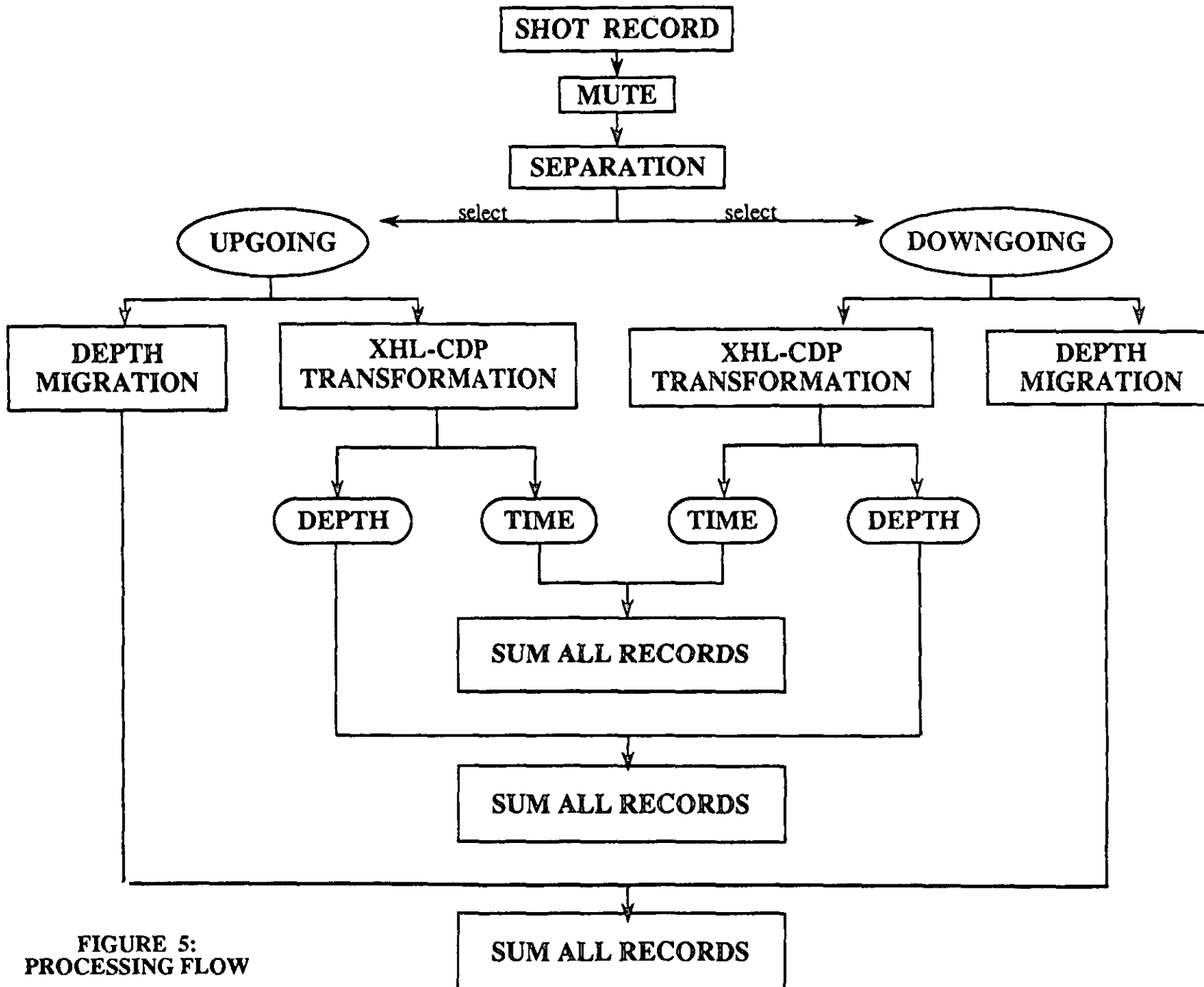
SHOT RECORD

MUTE

SEPARATION

select   select

UPGOING   DOWNGOING

DEPTH MIGRATION

XHL-CDP TRANSFORMATION

XHL-CDP TRANSFORMATION

DEPTH MIGRATION

DEPTH   TIME   TIME   DEPTH

SUM ALL RECORDS

SUM ALL RECORDS

SUM ALL RECORDS

232

FIGURE 5:
PROCESSING FLOW

3. Separation: After muting the direct arrivals , a 5-trace median filter was used to enhance the desired wavefield to process and reject the unwanted wavefield. Figure 6 shows examples of separated wavefields (after mute and separation) of shot 2 where both upgoing and downgoing waves were selected for processing. A detailed description of the median filtering process can be found in Hardage (1985) and Stewart (1985).

2-D f-k dip filtering was tested here for the wavefield separation of this data and produced unacceptable aliased noise and frequency artifacts.

4. Migration: The step after wavefield separation is migration of the selected waves, upgoing and downgoing, independently to their true reflection locations. Kirchhoff migration is used which consists of numerically calculating source and receiver wavefields at arbitrary times and depths from knowledge of the wavefields on a surface and then calculating coincidence of source and receiver wavefields to form an image. The form of Kirchhoff summation is derived in Wiggins (1983) and is the result of applying the Kirchhoff integral twice: once to extrapolate the receiver wavefield back to the reflection point, and again to extrapolate the source wavefield forward to the reflection point. This extrapolation produces a semielliptical trajectory with the source and receiver locations being the focal points. The previous procedure was one point on a trace. The same operation is performed for all points in all traces then superposition of all the resultant trajectories yields the migrated section. Wiggins and Levander (1984) explained the migration process for multiple offset synthetic VSP data.

Our depth migration results are shown in Figure 7 for the example of separated upgoing and downgoing waves (Figure 6). Kirchhoff migration of these separate wave types proves to be an accurate imaging of the subsurface reflectors present in our geologic model. A dip filter was applied internally in the migration process to reject events that have dips within 10 degrees of the raytraced structure dips. The same migration process is performed on the selected wavefields from the input shot records.

5. Crosshole-CDP transformation (XHL-CDP Transformation): As in VSP data, raw crosshole data in the depth and time domain are difficult to interpret in terms of lateral subsurface geology. The current study considers the VSP transformation technique (Wyatt and Wyatt, 1984; Dillon and Thomson, 1984) that reconstructs VSP data from the depth and time domain to surface distance (offset) and two-way (2-w) normal incidence time. In this method, a single time point is mapped from z-t domain to x-t_2 (t_2 is the 2-way normal incidence time) domain independent of the other points on the adjacent traces. Stewart (1988) derived the transformation formulae for the subsurface reflection point and the two-way vertical time in a constant velocity medium.

Our study interest in the previous studies is the ability to apply similar transformation process to crosshole reflected data and use its benefits in delineating the medium between the boreholes. Here, we call that mapping procedure XHL-CDP Transformation.

The formulae derived in Appendix A were used to investigate the subsurface-coverage geometry of the crosshole experiment. Figure 8 (a) demonstrates the covered subsurface zones for shot 2 (at depth 124 m). Note the extended coverage from the midpoint toward the source borehole for both upgoing and downgoing wavefields. In the multi-layered model case, this analysis still holds with slightly different subsurface locations due to ray bending.
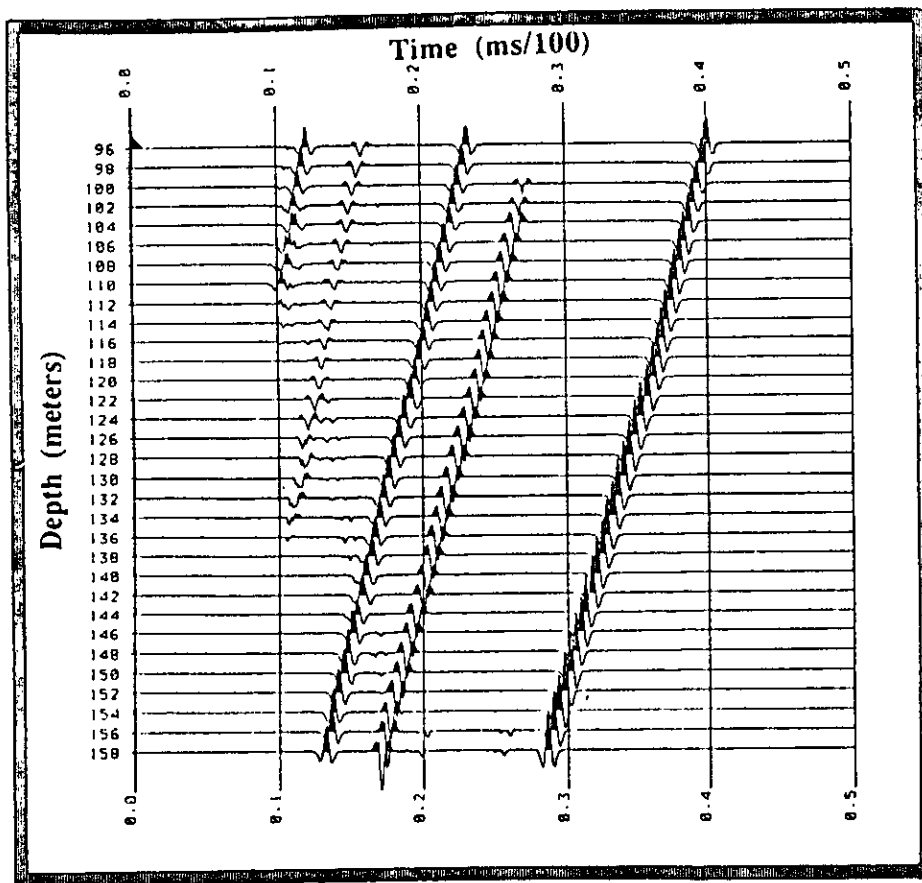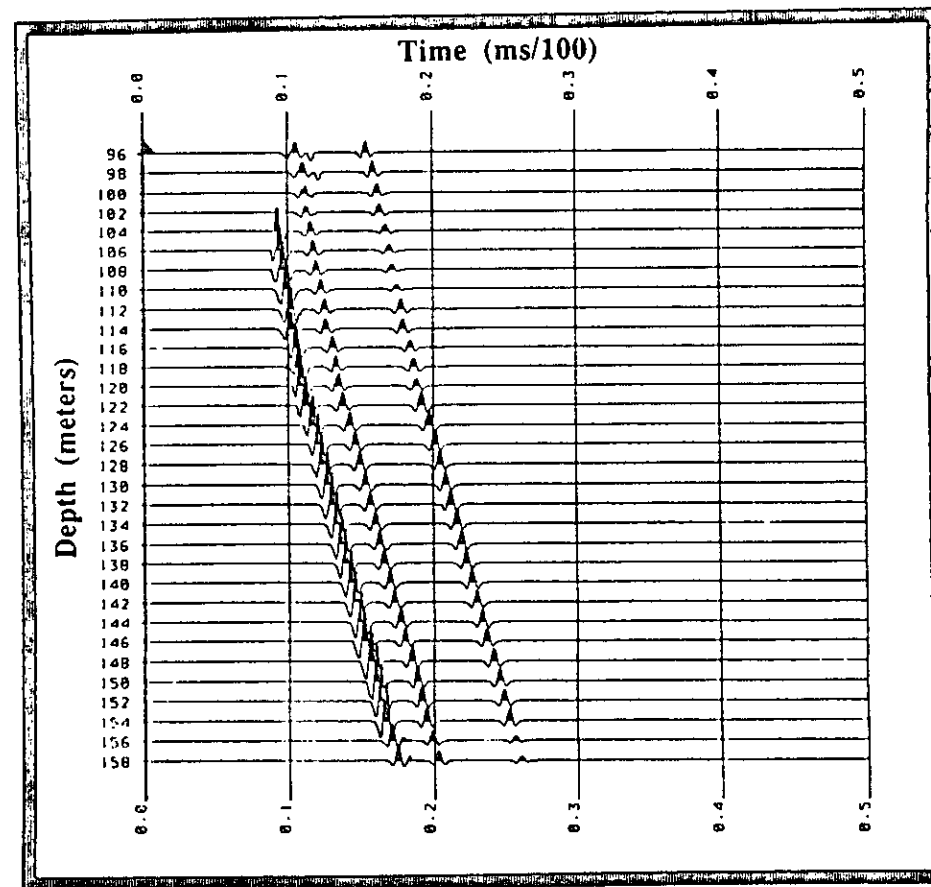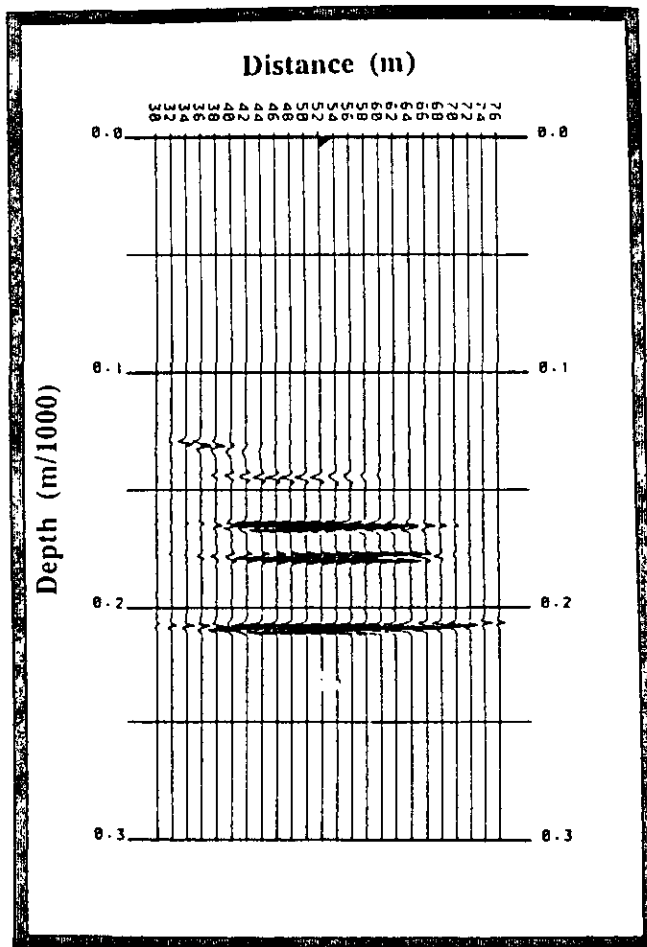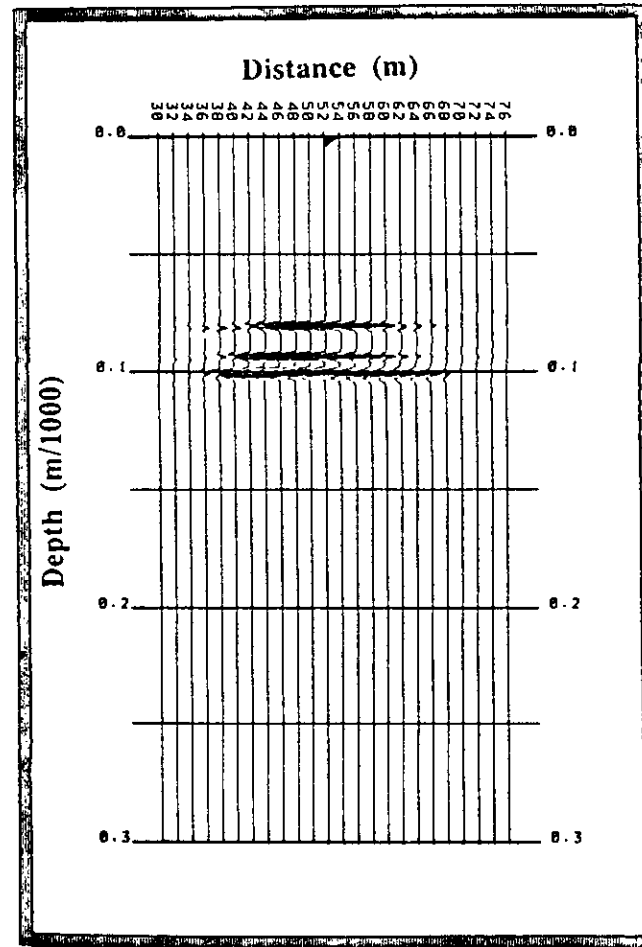
(a)   (b)

Figure 6: Shot 2 after mute and median filtering (separation). a) Reflected upgoing wavefield. b) Reflected downgoing wavefield.

Figure 7: Depth migration of both upgoing and downgoing reflected wavefields of shot 2. Events are located at their corresponding true model depths. a) Upgoing waves. b) Downgoing waves.
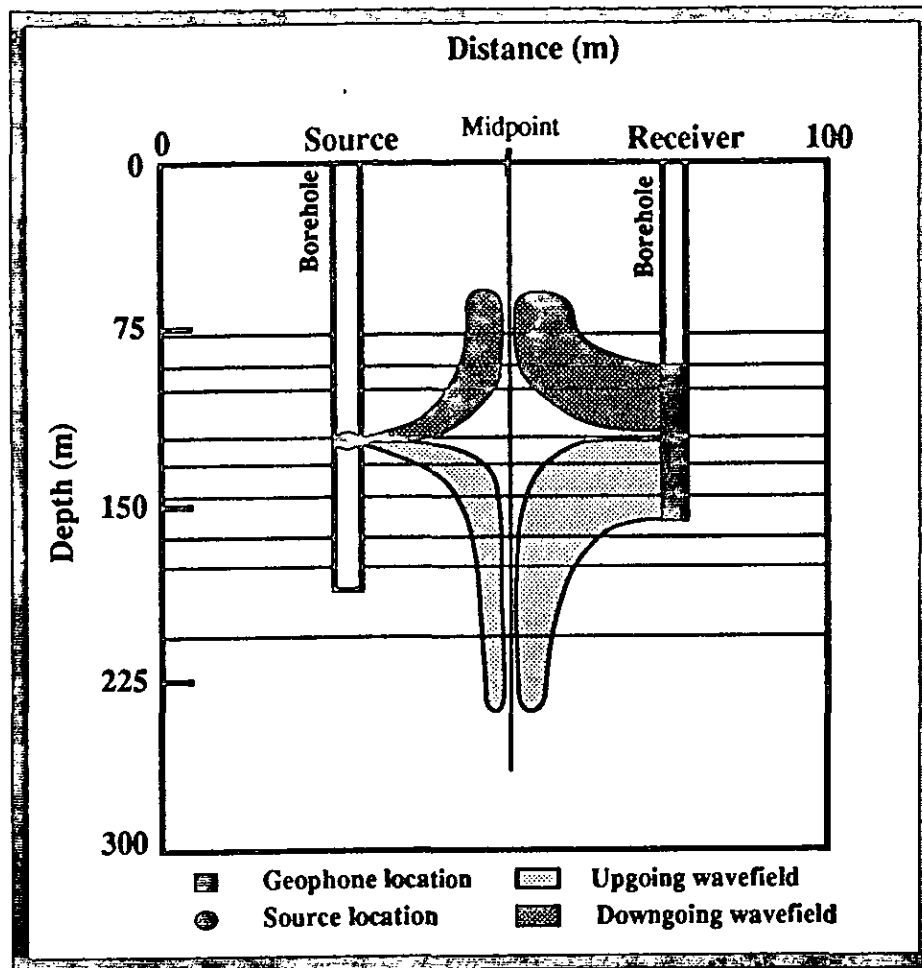
Figure 8 (a): Subsurface coverage for both upgoing and downgoing events in the case of shot 2. A constant-velocity medium is assumed here just to demonstrate the coverage geometry in the crosshole experiment.

In the current study, the constant-velocity assumption is eliminated by performing the correct mapping through a multi-layered raytracing. Figure 8 (b) shows a schematic example of a ray path following proper refractions that lead to the correct reflection point. From the known interval velocities in the background model, a time to depth conversion is easily performed to produce a depth section of the mapped area between the boreholes. An example of depth transformation (XHL-CDP Trans.) is presented in Figure 9. The data are again from shot 2 reflected upgoing and downgoing as the previous figures. The depth migrated sections (Figure 7) and depth transformed sections (Figure 9) compare nicely. The 2-way normal incidence time is shown in Figure 10 in which the same events in Figure 9 are converted into normal time from a datum, top of the model in this case.

6. Sum: Up to this stage, the processing was performed on individual records to obtain depth and time sections. The last step considered in this study is to sum the final records of the different wave types that are produced from the same process. This would give a final enhanced image containing the maximum subsurface coverage for both upgoing and downgoing wavefields. Figure 11 shows the three types of sections we considered above.
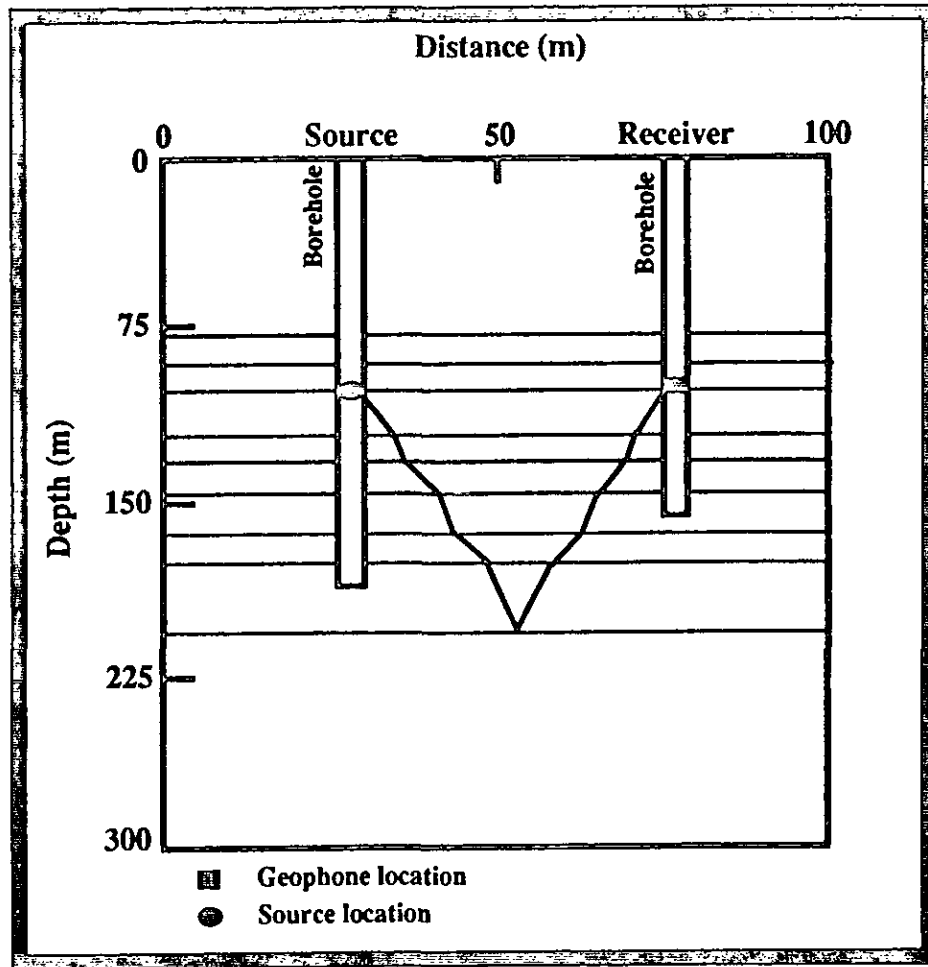
236

Figure 8 (b): A schematic ray trace through a multi-layered model that
would compute correct 2-w normal incidence time and subsurface reflection point.

Each section represents the sum of all reflected waves processed. The subsurface coverage
is very significant in that the horizon lateral continuity can be detected between the
boreholes. This type of information complements the interpretation of well logs where
only information around the boreholes is obtained. A second significant advantage is the
extension of the subsurface coverage away from the receiver borehole passing the
midpoint toward the source borehole where as the midpoint is the asymptote in the VSP
case.

CONCLUSIONS

Crosshole seismic data contains information that is less familiar to the seismic
exploration industry than VSP or surface seismic. This information represent reflected
wavefields in both upgoing and downgoing directions. The processing of such wavefields
does not need special software development. It can be performed using the conventional
borehole software currently available. A reconstruction technique that transforms
crosshole data from the depth and time of recording domain into surface distance and
subsurface depth domain was demonstrated. The multiple source/receiver gathers acquired
in the crosshole geometry can be used to obtain one enhanced image of the subsurface
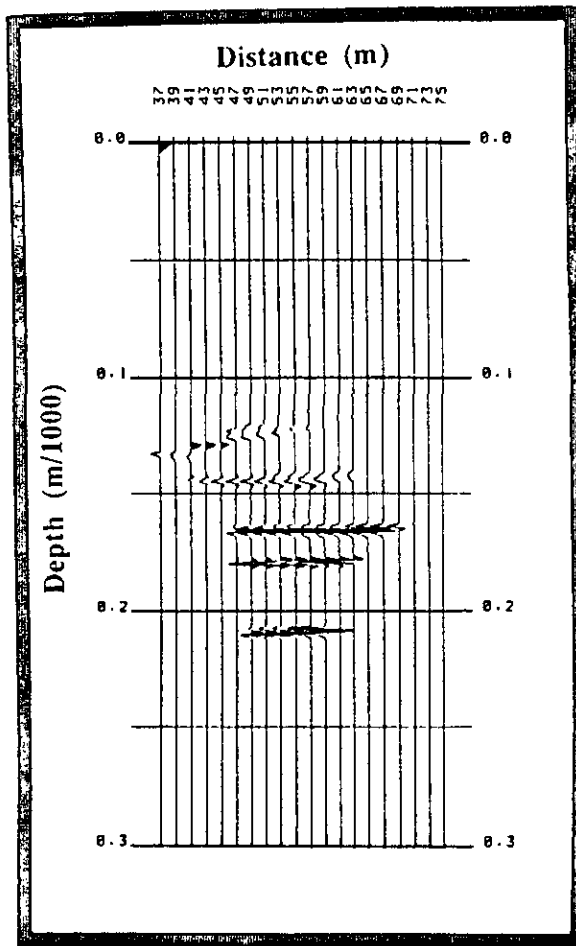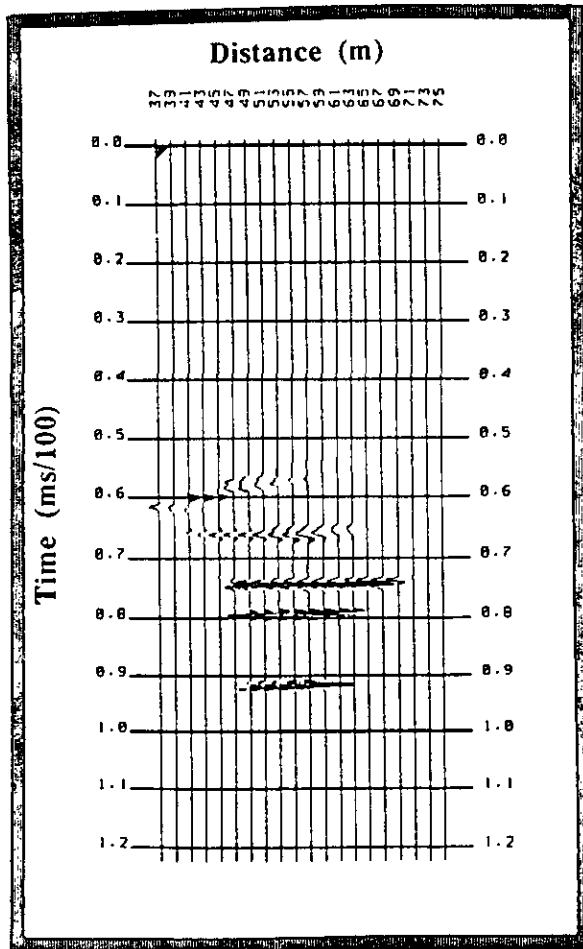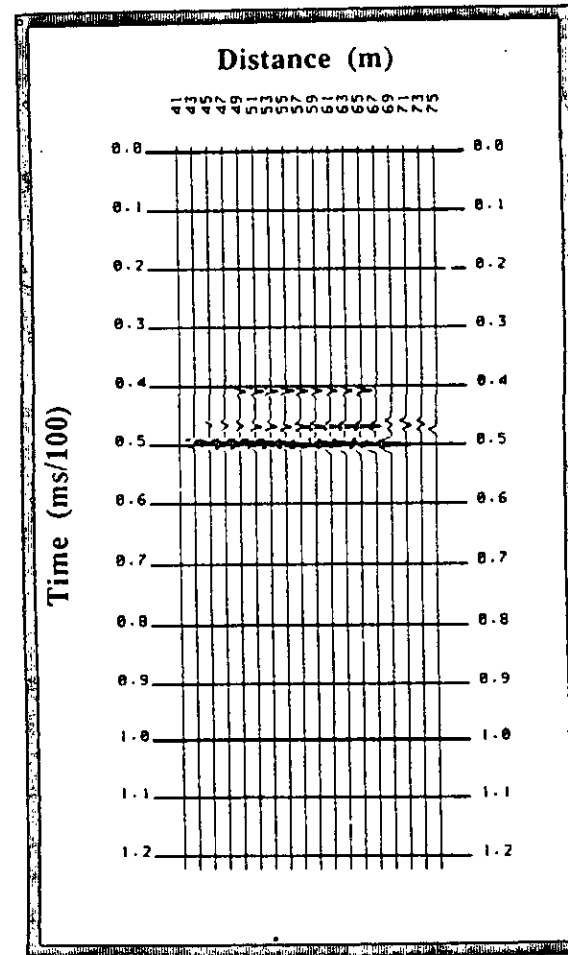
(a)
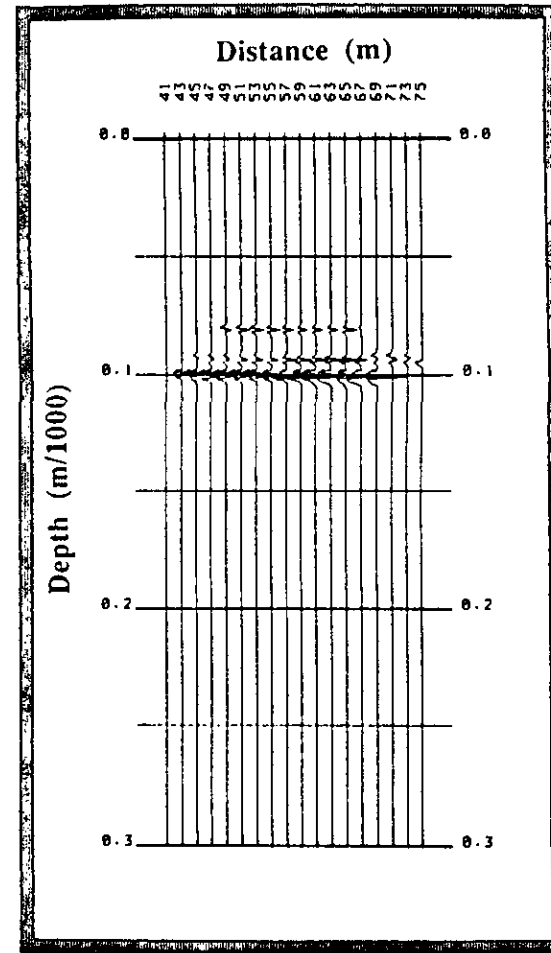
(b)

Figure 9: XHL-CDP Transformation in depth for both upgoing and downgoing reflected wavefields of shot 2. a) Upgoing waves. b) Downgoing waves. There is an excellent comparison between depth migrated sections (Fig. 7) and depth transformed sections (this figure) in terms of depth not offset.
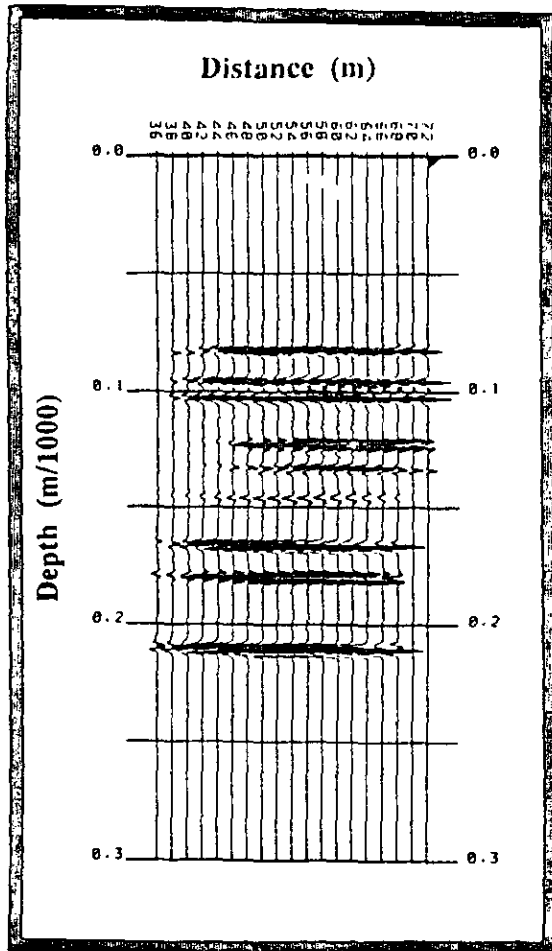
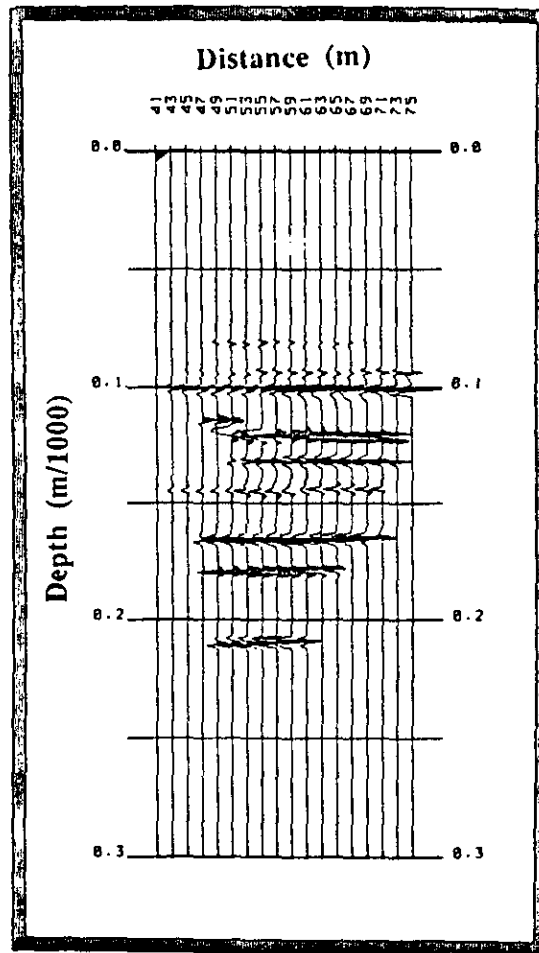(a)   (b)
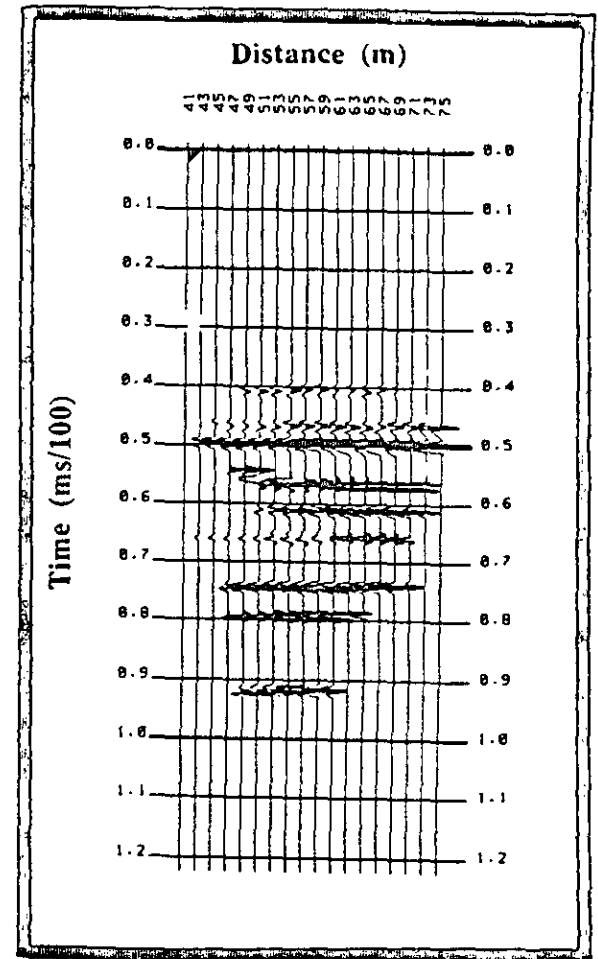
Figure 10: XHL-CDP Transformation in time for both upgoing and downgoing reflected
wavefields of shot 2. a) Upgoing waves. b) Downgoing waves. The time displayed here is the
two-way normal incidence time from the datum, top of the model in this case, to each depth level.

(a)

(b)

(c)

FIGURE 11: The sum of all waves, upgoing and downgoing, of the same data type for the subsurface area between the borehole. a) Depth migration. b) Depth transformation. c) Time transformation. Depth (migration and transformation) events are very well comparable. Note the extended subsurface coverage of the total-wave sum over independent shot coverage.

medium between the boreholes. The coverage obtained from the multi-source experiment extends away from the borehole and can be used to detect the subsurface lateral continuity between the boreholes to complement other borehole experiments as well logging and Vertical Seismic Profiling (VSP).

FUTURE WORK

The next step in studying the processing of crosshole data is to consider physical model and real field data. A number of problems will likely present themselves (such as tube waves and source directivity). Other preprocessing steps will have to be carefully studied. For example, gaining and deconvolving real data.

Acknowledgments:

The authors of this paper wish to thank Shell Canada, and Dr. David Henley in particular, for providing the log and crosshole data. The processing presented here was conducted at Western Geophysical Company, Canada. Many thanks to Roger Hawthorne, Bill Rimmer, Adam Chow and Lynn Burroughs of Western Geophysical for their generous assistance. Last and definitely not least, thanks to all the sponsors of the CREWES Project for the continuous support.

REFERENCES

Baker, L. J., and Harris, J. M., 1984, Cross-Borehole Seismic Imaging: paper BHG2.2 presented at the 1984 Annual Meeting of SEG, Atlanta, Dec. 2-6.

Beydoun, W. B., Delvaux, J., Mendes, M., Noual, G., and Tarantola, A., 1988, Practical Aspects of an Elastic Migration/Inversion of Crosshole Data For Reservoir Characterization: A Paris Basin Example: Personal communications (In Press).

Bregman, N. D., Hurley, P. A., and West, G. F., 1989, Seismic tomography at a fire-flood site: Geophysics, 54, 1082-1090.

Dillon, P. B., and Thomson, R. C., 1984, Offset source VSP surveys and their image reconstruction: Geophys. Prosp., 32, 790-811.

Hardage, B. A., 1985, Vertical Seismic Profiling: Geophysical Press, 14A.

Hu, L., McMechan, G. A., and Harris, J. M., 1988a, Acoustic prestack migration of cross-hole data: Geophysics, 53, 1015-1023.

Hu, L., McMechan, G. A., and Harris, J. M., 1988b, Elastic finite-difference modeling of cross-hole seismic data: Bull. Seis. Soc. Am., 78, 1796-1806.

Ivansson, S., 1985, A study of methods for tomographic velocity estimation in the presence of low-velocity zones: Geophysics, 50, 969-988.

Iverson, W. P., 1988, Crosswell Logging for Acoustic Impedance: Pet. Tech. J., 75-82.

Macrides, C. G., 1987, Seismic tomography in oil sands for monitoring thermal recovery processes: Ph. D. thesis, Physics Department, University of Alberta.

Seeman, B., and Horowicz, L., 1983, Vertical seismic profiling: Separation of upgoing and downgoing acoustic waves in a stratified medium: Geophysics, 48, 555-568.

Stewart, R. R., 1988, VSPCDP Map for P waves: Personal communications (in Press).

Stewart, R. R., 1985, Median filtering: Review and a new f/k analogue design: J. Can. Soc. Expl. Geophys., 21, 54-63

Wiggins, J. W., 1984, Kirchhoff integral extrapolation and migration of nonplanar data: Geophysics, 49, 1239-1248.

Wiggins, J. W., and Levander, A. R., 1984, Migration of multiple offset synthetic vertical seismic profile data in complex structures: in Simaan, M., Ed., Advances in Geophysical data Processing, 1, JAI Press, Greenwich, CT., 269-290.

Wyatt, K. D., and Wyatt, S. B., 1984, Determining subsurface structure using the vertical seismic profiling: In Toksoz, M. N., and Stewart, R. R., Eds, Vertical seismic profiling: Advanced concepts, Geophysical Press.

Yilmaz, O., 1987, Seismic data processing: Soc. Expl. Geophys., 252-260.

Zhu, X., and McMechan, G. A., 1988, Acoustic modeling and migration of stacked cross-hole data: Geophysics, 53, 492-500.

APPENDIX A

Crosshole (XHL)-CDP Transformation in a constant-velocity model

Consider the geometry shown in Figure 12. A source S located at depth s in a borehole and a receiver H is placed in another borehole at depth h. X is the distance between the source and the receiver boreholes. Point H' is the image point for receiver H with respect to a reflector R, with depth r from the surface. Point S' is at the same depth level as point S (the source). The problem is stated as follows;
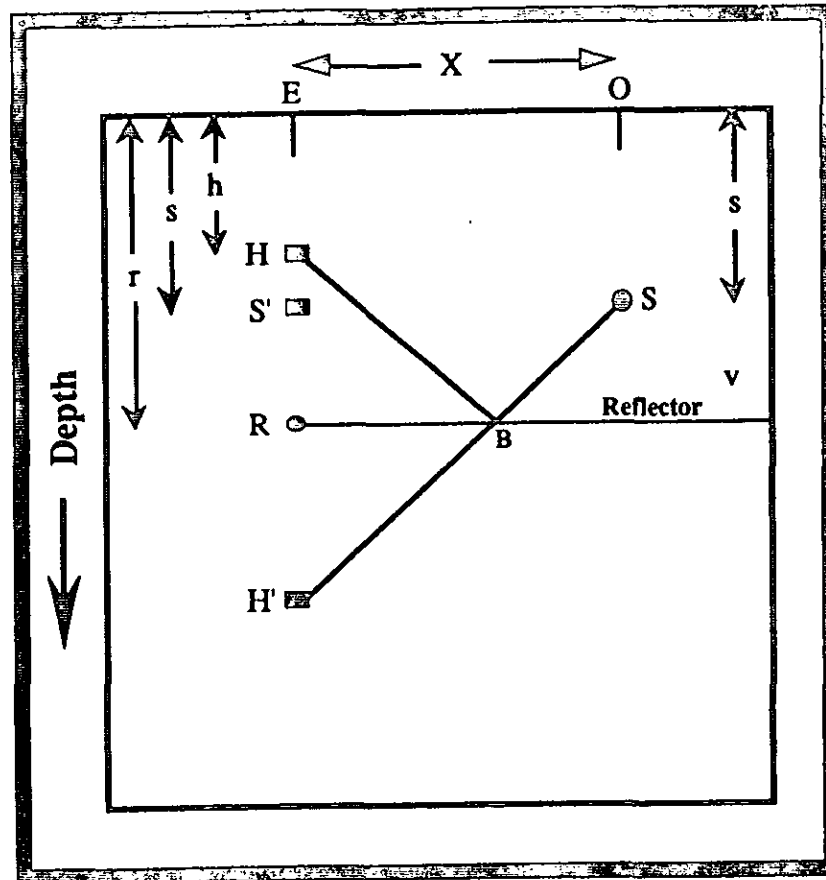

Figure 12: A constant- velocity case to derive the 2-way normal incidence time and subsurface reflection point

Knowing the travel time from the source to a receiver, the depths of the source and that receiver and the distance between the borehole, can we map crosshole traveltimes into two-way vertical time and reconstruct the sample points in their subsurface locations where they reflected from ?

The following derivation hopes to answer this question for the geometry considered in Figure 12. The method follows Stewart (1988) scheme for VSPCDP map of P-waves. For source S and receiver H,

The total length of the ray

$$SBH = \left[(2r-h-s)^2 + x^2\right]^{\frac{1}{2}}$$

$\Rightarrow$ The traveltime of the ray t,

$$t = \frac{\left[(2r-h-s)^2 + x^2\right]^{\frac{1}{2}}}{v}$$

by squaring both sides of the equation and solving for r

$$r = \frac{1}{2}\left[(t^2 v^2 - x^2)^{\frac{1}{2}} + h + s\right]$$

$\Rightarrow$ The two-way vertical time t_v,

$$t_v = 2\frac{r}{v}$$

$\Rightarrow$

$$t_v = \left(t^2 - \frac{x^2}{v^2}\right)^{\frac{1}{2}} + \frac{h+s}{v}$$

Now, to find where the reflection point B is with respect to the receiver borehole we use similar triangles:

$$\frac{BR}{X} = \frac{RH'}{S'H'} \qquad (BR = X_B)$$

$\Rightarrow$

$$X_B = X\left[\frac{r-h}{2(r-h)-(s-h)}\right]$$

after some algebra,

$$X_B = \frac{X}{2}\left[1 + \frac{s-h}{(t^2 v^2 - X^2)^{\frac{1}{2}}}\right]$$

or $\left(\text{by } r = \frac{v\, t_v}{2}\right)$

$$X_B = \frac{X}{2}\left[\frac{v\, t_v - 2h}{v\, t_v - h - s}\right]$$

These formulae are applicable for all receivers and sources located above the interface where reflections may occur. If the receiver has the same depth as the source (s=h), then the formulae become

$$t_v = \left(t^2 - \frac{x^2}{v^2} \right)^{\frac{1}{2}} + \frac{2\,h}{v}$$

· and

$$X_B = \frac{X}{2}$$

As we can see, these formulae are only adequate for a constant velocity medium. Nevertheless, the only two previous studies that considered crosshole mapping (Baker and Harris, 1984; Iverson, 1988) used a constant velocity model. This would be adequate only if the velocity contrasts are not very high. In the presence of low-velocity producing zones and if the assumed velocity was higher than the true velocity, the mapped events are going to be shifted up in their 2-way normal time and also the reflection point locations are not going to be correctly computed.